scientific reports

OPEN

Detection of volatile organic compounds using mid-infrared silicon nitride waveguide sensors

Junchao Zhou[1], Diana Al Husseini[2], Junyan Li[1], Zhihai Lin[1], Svetlana Sukhishvili[2], Gerard L. Coté[3], Ricardo Gutierrez-Osuna[4] & Pao Tai Lin[1,2]✉

Mid-infrared (mid-IR) sensors consisting of silicon nitride (SiN) waveguides were designed and tested to detect volatile organic compounds (VOCs). SiN thin films, prepared by low-pressure chemical vapor deposition (LPCVD), have a broad mid-IR transparent region and a lower refractive index ($n_{SiN} = 2.0$) than conventional materials such as Si ($n_{Si} = 3.4$), which leads to a stronger evanescent wave and therefore higher sensitivity, as confirmed by a finite-difference eigenmode (FDE) calculation. Further, in-situ monitoring of three VOCs (acetone, ethanol, and isoprene) was experimentally demonstrated through characteristic absorption measurements at wavelengths $\lambda = 3.0$–3.6 μm. The SiN waveguide showed a five-fold sensitivity improvement over the Si waveguide due to its stronger evanescent field. To our knowledge, this is the first time SiN waveguides are used to perform on-chip mid-IR spectral measurements for VOC detection. Thus, the developed waveguide sensor has the potential to be used as a compact device module capable of monitoring multiple gaseous analytes for health, agricultural and environmental applications.

Detection of VOC is critical for a variety of applications, ranging from health diagnostics to environmental and industrial monitoring[1–5]. Two general approaches are often used for VOC analysis, one based on analytical techniques such as gas chromatography mass spectrometry (GC–MS)[6,7], and another involving solid-state sensors, based on metal-oxide semiconductors (MOS)[8–10], electrochemical (EC)[11] or photoionization detection (PID)[12]. GC–MS can provide accurate gas analysis, but the systems are bulky and thus unsuitable for point-of-use (POU) and real-time applications. In turn, solid-state chemical sensors can have high sensitivity and portability, but have low selectivity to discriminate among VOCs. As an alternative to conventional solid-state sensors, mid-IR sensing can provide high selectivity by measuring absorption of the characteristic and finger-print vibrational features of VOCs. However, mid-IR absorption spectroscopy requires bench-top optical equipment such as Fourier-transform infrared spectroscopy (FTIR), which is unpractical for POU applications[13,14]. To address this issue, miniaturized photonic circuits consisting of optical waveguides and other chip-scale photonic components have been explored[15–17]. However, prior approaches have used waveguide materials that have high refractive indices, such as Si and Ge[18,19], which lead to a weak evanescent wave[20,21] and therefore poor sensitivity. Chalcogenide materials have also been used[22], and they provide stronger evanescent fields, but they are prone to degradation upon exposure to moisture, thus requiring storage under dry N_2 or high vacuum condition.

To address this issue, the present study examines the use of SiN as the waveguide material. SiN has a low refractive index ($\mathbf{n_{SiN}} = 1.94$) compared to Si ($\mathbf{n_{Si}} = 3.4$), which leads to a strong evanescent wave and therefore higher sensitivity, and also possesses exceptional chemical stability and can be repeatedly used in ambient humidity conditions[23,24]. Further, SiN has a broad infrared transparency window, low optical loss, and high compatibility with complementary metal-oxide-semiconductor (CMOS) processes[25,26]. These properties make SiN an ideal material for waveguide sensors to enable repeatable, reproducible VOCs detection over long-term sensing operation. To our knowledge, however, prior work on SiN as a waveguide material has been primarily theoretical or has focused on wavelength sensing in the visible range, rather than the far more informative mid-IR range[27–29].

To demonstrate the potential of SiN waveguide sensing for mid-IR detection of gaseous analytes, we focused on three VOCs (acetone, ethanol, and isoprene) that are potential biomarkers for breath analysis. For instance, exhaled acetone has been studied to monitor diabetic ketoacidosis[30,31], ethanol for alcohol abstinence[32], and

[1]Department of Electrical and Computer Engineering, Texas A&M University, College Station, TX 77843, USA. [2]Department of Materials Science and Engineering, Texas A&M University, College Station, TX 77843, USA. [3]Department of Biomedical Engineering, Texas A&M University, College Station, TX 77843, USA. [4]Department of Computer Science and Engineering, Texas A&M University, College Station, TX 77843, USA. ✉email: paolin@ece.tamu.edu
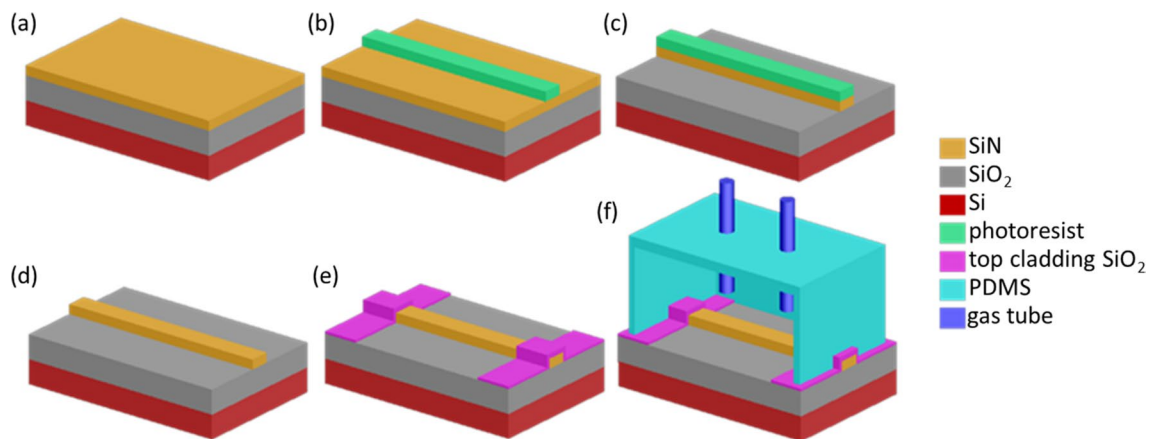
Figure 1. Fabrication process of the SiN waveguide and its assembly with a PDMS chamber. (**a**) Deposition of SiN thin film by LPCVD. (**b**) Creation of waveguide patterns by photolithography. (**c**) Transfer of the waveguide pattern to the SiN layer by RIE. (**d**) Removal of photoresist. (**e**) Deposition of the top SiO_2 cladding layer. (**f**) Bonding of the PDMS chamber to the waveguide sensor.

isoprene for lung cancer and high blood cholesterol[33,34]. Further, these VOCs have strong mid-IR absorption signatures at wavelengths between 3.0–3.6 μm, which are detectable using the proposed SiN photonic circuits. Being compatible with CMOS fabrication processes, the proposed SiN mid-IR waveguide sensor offers the potential for a compact device platform to realize real-time gas analysis.

Experimental methods

Fabrication of SiN waveguide sensor and gas chamber. Figure 1a–f illustrates the fabrication of mid-IR SiN waveguides, along with a polydimethylsiloxane (PDMS) chamber for VOC detection. In step (a), a low-stress SiN thin film with thickness $T = 1$ μm was deposited on a Si wafer by LPCVD. The grown Si-rich SiN has a low tensile stress of 45 MPa. A 3 μm thick thermo-oxide acts as the low-refractive-index under-cladding layer between the SiN and the Si. In step (b), the pattern of waveguides was generated on top of the SiN thin film via photolithography (Karl Suss MA-6 mask aligner). The waveguide pattern was then transferred into the SiN thin film layer in step (c) using reactive ion etching (RIE). After removing the photoresist in step (d), a 3 μm thick SiO_2 layer was deposited on both sides of the SiN waveguide by plasma-enhanced chemical vapor deposition (PECVD). The center of the waveguide was left open for VOC detection, as shown in step (e). The length of the waveguide sensing region, where the mid-IR evanescent wave interacted with the VOCs, is 8 mm long. A PDMS (Dow Corning Sylgard 184) chamber was prepared by dropping the PDMS precursor into a customized mold. In step (f), the molded PDMS was bonded to the SiN waveguide device to form a sealed gas chamber. The 8 mm long sensing region is an ideal length to integrate with the PDMS chamber providing high gas sealing. The top SiO_2 layer patterned in step (e) eliminates direct contact between the PDMS chamber and the SiN waveguides to prevent absorption by PDMS from interfering with the sensing measurement.

Setup for SiN waveguide characterization and VOC absorption measurement. Figure 2 shows a schematic of the experimental set-up for waveguide characterization and VOC detection via a fiber-waveguide-fiber configuration. A tunable mid-IR laser (M Squared Firefly) with 150 kHz pulse repetition rate, 10 ns pulse duration, and 150 mW average power, was used as the light source. The wavelength tuning range of the laser was from 2.5 to 3.7 μm. The laser light was coupled into a single mode ZrF_4 fiber (Thorlabs) through a reflective lens collimator (RL) and then butt-coupled to the SiN waveguide. The fine position adjustment between the fiber and the waveguide was monitored with an optical microscope. The coupling loss was 5.2 dB and the waveguide loss was 2.1 dB/cm at 3.5 μm wavelength.

Three VOCs (acetone, ethanol, and isoprene) were used as the analytes. VOC vapors were prepared by flowing nitrogen gas through bottles with VOCs in liquid form. The flow rates of the VOC vapors and the nitrogen carrier gas were regulated by mass flow controllers (MFCs). The gas phase analyte was delivered into the sealed PDMS chamber with the waveguide sensor inside. The gas pressure into the PDMS chamber was monitored by the mass flow controllers and pressure regulators. The temperature of the system was maintained at room temperature 20 °C. The intensity of the waveguide light was attenuated according to the mid-IR absorption spectra of the VOCs. Light propagating through the waveguide was collected by a multimode ZrF_4 fiber with a 400 μm core diameter (Thorlabs). The fiber was connected to a photodetector (Thorlabs PDA20H), and the light intensity was read by a digital multimeter and recorded in a computer.

Results and discussion

Characterization of SiN waveguides and VOCs absorption measurement. Figure 3a shows the fabricated SiN waveguide sensor with the attached PDMS gas chamber. The input and output waveguides were placed out of line with an offset of 5 mm to minimize contributions from background light that was not coupled
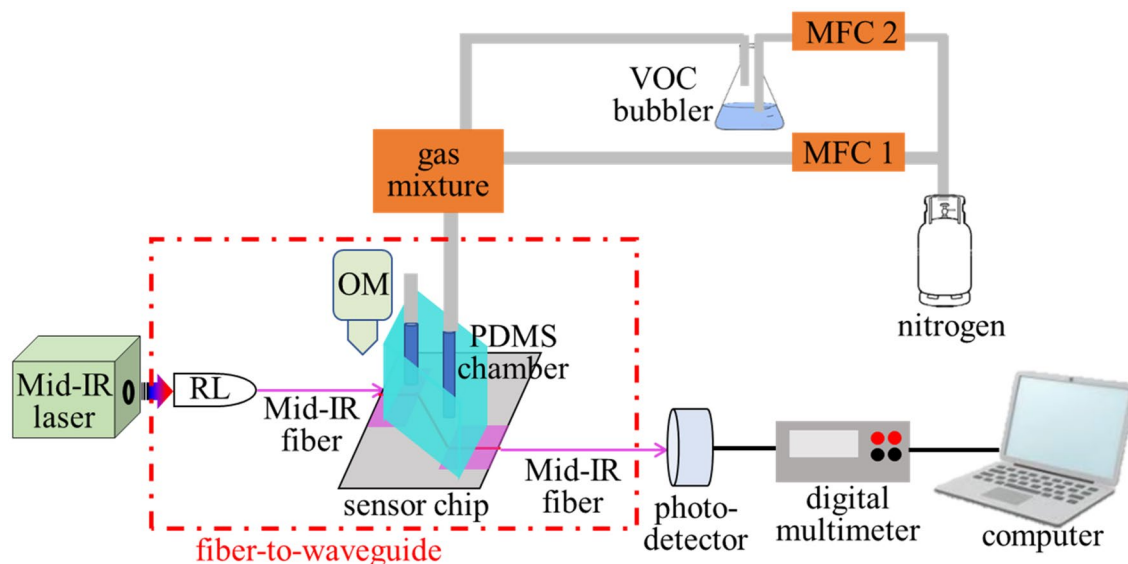
Figure 2. Experimental setup of the VOC detection measurement. Mid-IR probe light from the laser was coupled into the waveguide using a butt-coupling method. The guided light was collected by another fiber after the waveguide end-facet. VOC vapor was carried by N_2. The flow rate the VOC concentration were controlled by the MFCs.
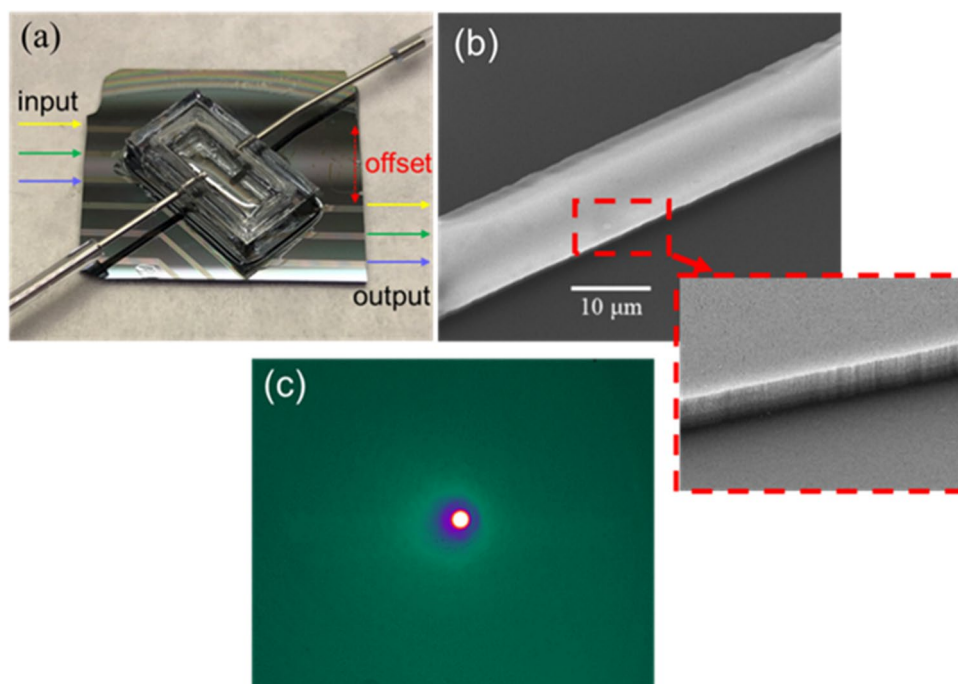

Figure 3. (**a**) Sensor device with SiN waveguides and PDMS chamber. Input and output waveguides were offset by 5 mm. (**b**) SEM top image of a SiN waveguide. The zoom-in tilted image shows its side wall. (**c**) The mode image from a single SiN waveguide.

into the waveguide. Figure 3b is an SEM image of the SiN waveguide and its die wall. The waveguide width is 10 μm. The reason of using the 10 μm wide waveguide is to improve the coupling efficiency between the 9 μm core-diameter fiber and the SiN waveguide. Both the waveguide top surface and side wall are smooth, as depicted in Fig. 3b. Figure 3c shows the waveguide mode of the SiN waveguide captured at λ = 3.3 μm by a liquid-nitrogen cooled mid-IR camera (IRC 800 series, IRcameras). A sharp spot corresponding to a single fundamental waveguide mode was observed, and no scattering was found in the entire field of view. This indicates that the input light was well confined within the SiN waveguide, and that the background light in the substrate

layer was minimized by the off-set design. Specifically, the width of the fabricated waveguide is 10 μm, which is close to the single mode mid-IR fiber with a 9 μm diameter. Therefore, the waveguide mode excitation efficiency for the fundamental mode is larger than the higher-order modes because the fundamental mode has a better spatial overlap with the fiber's single-mode. As a result, the experimentally observed waveguide mode showed a fundamental mode dominant profile. Our LPCVD Si-rich SiN also has low optical loss of 0.2 dB/cm and low tensile stress of 45 MPa for a film thickness of 2 μm.

Finite-difference eigenmode (FDE) analysis of waveguide modes and mid-IR sensitivity.   Mode profiles of the SiN and Si waveguides and their sensitivities were calculated using FDE, which allowed us to evaluate the sensitivity of mid-IR waveguides made of different materials and structures. Figure 4a–d shows the 2-D waveguide modes for various waveguide structures at λ = 3.3 μm, and Fig. 4e–h displays the corresponding 1-D light intensity and refractive indexes distributions along the z-axis at x = 0 μm. The waveguides had the same width of 10 μm. Two different waveguide thicknesses of T = 1 μm and 2 μm were considered for the transverse magnetic (TM) polarization. Waveguide sensing performance was evaluated by comparing the evanescent field intensity distribution for the two waveguides. The T = 1 μm Si waveguide showed a weak evanescent field extending to the outer medium (z > 1 μm), while the T = 1 μm SiN waveguides showed a strong evanescent field outside of the waveguide. The intensity profile remained the same in the *x* direction. As the thickness of the waveguide increased to T = 2 μm, the intensity of the evanescent field significantly decreased for both the SiN and Si waveguides, as illustrated in Fig. 4c,d, respectively. However, the SiN waveguide still showed a stronger field than the Si waveguide.

The FDE method was also used to analyze the sensitivity of the mid-IR waveguides. The sensitivity of the waveguide is defined as the attenuation of the waveguide intensity, which is equivalent to the waveguide propagation loss per unit length, upon exposure to an external medium. Here, the external medium is the VOC analyte and it has a homogeneous refractive index profile. The real part of the refractive index of the external medium is 1 and the imaginary part is determined by the absorption coefficient of the VOC. The relative sensitivity was then calculated by comparing its value with the sensitivity at T = 1.0 μm. The wavelength in the simulation is λ = 3.375 μm. As shown in Fig. 5, the sensitivity was improved by 5.1 times as the thickness T decreased from 2 to 0.8 μm. This was because the evanescent field extended into the VOC analyte increased at the thinner waveguide thickness. The sensitivity decreased at T < 0.8 μm because such a thin waveguide no longer supported the waveguide mode. The sensitivity vs. wavelength was also investigated and illustrated in Fig. 6. The change of sensitivity was almost negligible for both waveguide materials across the 3.2–3.5 μm wavelength range, indicating the waveguide sensors have uniform performance over a broad spectrum, which is critical for mid-IR VOCs analysis.

Real-time VOC detection and absorption spectrum characterization.   Figure 7 shows real-time VOC detection using the mid-IR SiN waveguide sensor illustrated in Fig. 2. The SiN waveguide had a width of 10 μm and a thickness of 1 μm. The waveguide thickness, T, was optimized and fixed to 1 μm for both the Si and SiN waveguides due to the limitation in coupling from the large 9 μm core fiber. A waveguide thinner than 1 μm will decrease the fiber-to-waveguide butt-coupling efficiency, since presently there is no conventional mid-IR lensed fiber available. Although other coupling approaches such as on-chip light sources and off-axis parabolic mirror are under development, this butt-coupled fiber optic approach is what is currently commercially available with high coupling efficiency. During the measurement, pure nitrogen was first injected into the PDMS chamber, and the waveguide intensity obtained was defined as the baseline. Once the waveguide intensity stabilized, VOC vapor was injected into the PDMS chamber until the waveguide intensity stabilized. Each measurement was repeated for 3–4 cycles of VOC injection and nitrogen purging to ensure the results were consistent and repeatable. The transient response during the acetone, ethanol, and isoprene measurements are plotted in Fig. 7a–c, respectively, and showed a deviation over time within 1% for each of the gases.

The vibrational bands caused by the C–H stretching vibrations for acetone are 3.305 μm with A1 symmetry and 3.168 μm with F2 symmetry. For ethanol, there are symmetric stretching vibration at 3.412 μm and symmetric stretching vibration at 3.364 μm. For acetone and ethanol vapor, the waveguide light intensity decreased over time when their vapor flowed into the chamber and then reached an equilibrium state after 10–20 s, indicating that the VOC molecules steadily attached to the waveguide surface. Once the nitrogen was reinjected into the chamber, the waveguide intensity increased and recovered to its initial intensity level within 20 s. For isoprene, the waveguide light intensity dropped nearly instantaneously once the isoprene vapor was injected due to its high volatility.

These results indicate that the SiN waveguide can detect different VOCs and measure their transient response. Unlike chalcogenide waveguides, SiN has high chemical stability and resistance to moisture, so the SiN waveguide sensor does not demonstrate signal degradation and can be used for long-term repeatable VOCs monitoring. The absorption spectrum of VOCs can be calculated using the real-time measurement according to the Beer's law equation $A = -\log(I/I_0)$, where A is the absorbance, and I and I_0 are the waveguide intensities with and without the VOC, respectively. The spectra of acetone, ethanol and isoprene measured by the SiN waveguide are plotted in Fig. 8a–c, where the absorbance in y-axis is normalized to its maximum. Note that the spectra are not meant to show the ability to separate these gas molecules spectrally but rather to show that the characteristic absorption bands caused by the C–H stretching vibrations between λ = 3.1 and 3.6 μm could be observed. The spectral features were consistent with FTIR spectra (NIST WebBook) shown in Fig. 8d–f, though the resolution of our tunable laser was not as high. For instance, the major absorption peak at λ = 3.35 μm was depicted for acetone and at 3.4 for μm ethanol for our system. In addition, the two broader isoprene absorption peaks at λ = 3.25 and 3.4 μm were observed in both systems. Figure 9 shows the relative absorbance of acetone using a Si waveguide, compared to the results obtained using the SiN waveguides. Both Si and SiN waveguides were 10 μm wide and
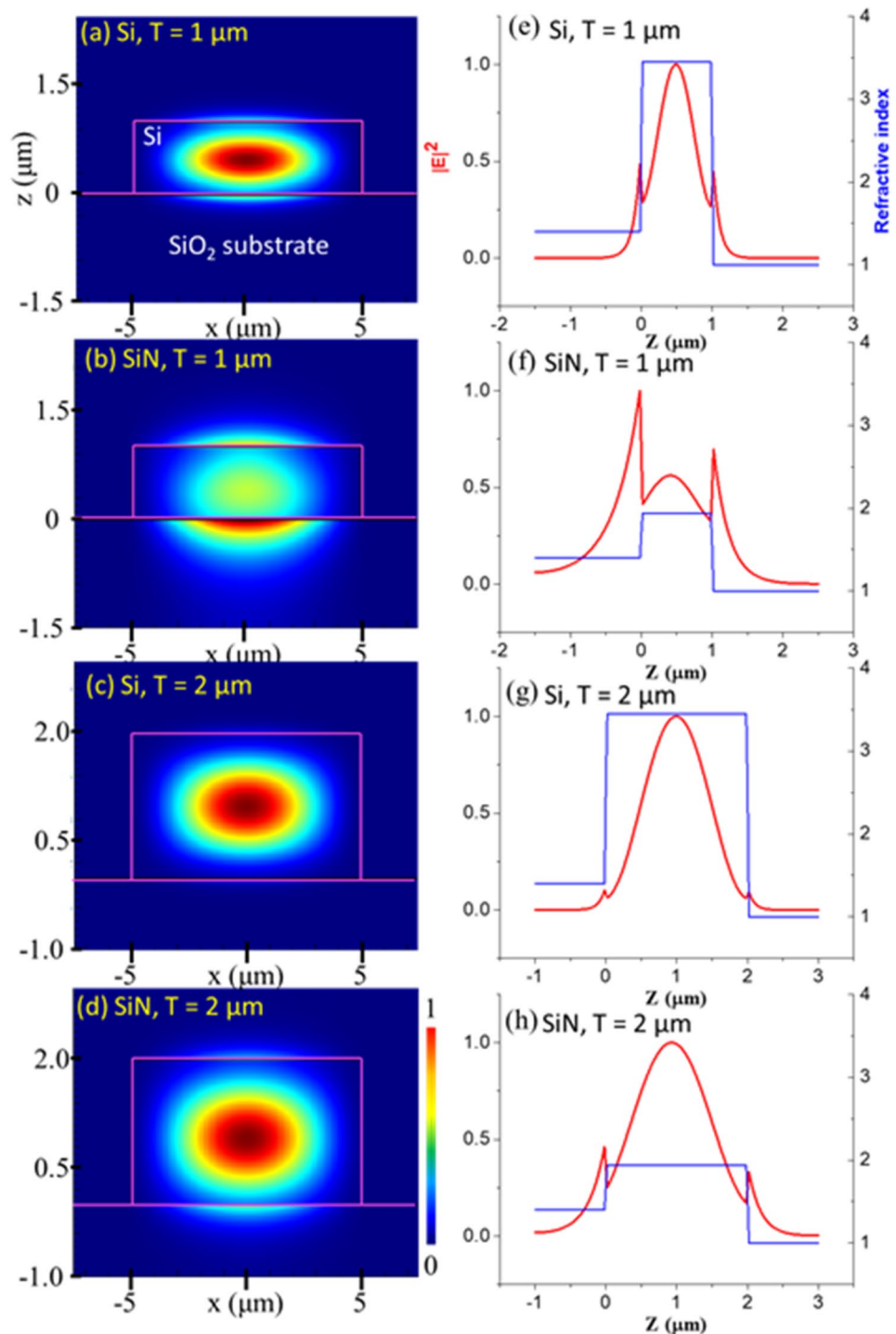
Figure 4. (**a–d**) Simulated 2-D waveguide modes and (**e–h**) 1-D intensity profiles along the z-axis for thicknesses T = 1 and 2 μm for the Si and SiN waveguides, respectively. TM polarization was selected for the waveguide modes.

1 μm thick in these experiments. The results of Fig. 9 experimentally confirm the primary result anticipated from the FDE modeling, showing that attenuation (and therefore sensitivity) in the SiN waveguide is five times stronger than that of the Si waveguide.

Figure 10 shows the relative absorbance with relative concentration of the individual VOCs. Gas concentration was controlled by adjusting the flow rates of MFC 1 and MFC 2; see Fig. 2. The x-axis in Fig. 10 is the ratio of flow rates: (MFC2)/(MFC1 + MFC2). We observe a monotonic increase in relative absorbance with VOC concentration, which is fairly linear below a ratio of 0.7 and then follows a nonlinear increase at higher ratios. The
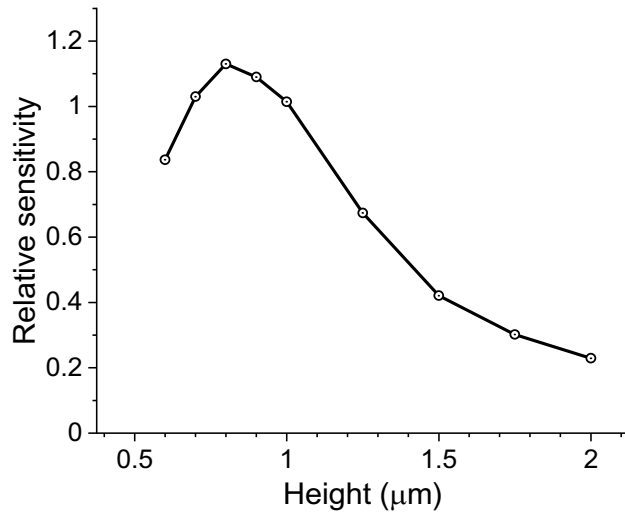
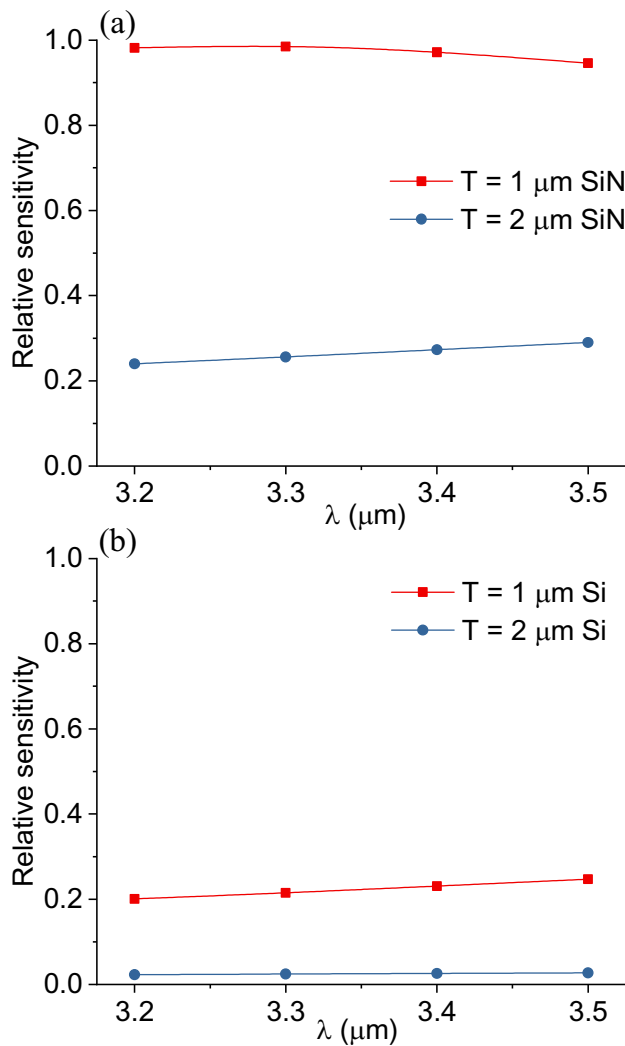**Figure 5.** Sensitivity vs waveguide thickness T at **n** = 2, which corresponds to the SiN material.

Figure 6. Sensitivity vs wavelength (λ) for (**a**) SiN and (**b**) Si waveguides at thicknesses T = 1 and 2 μm, respectively.
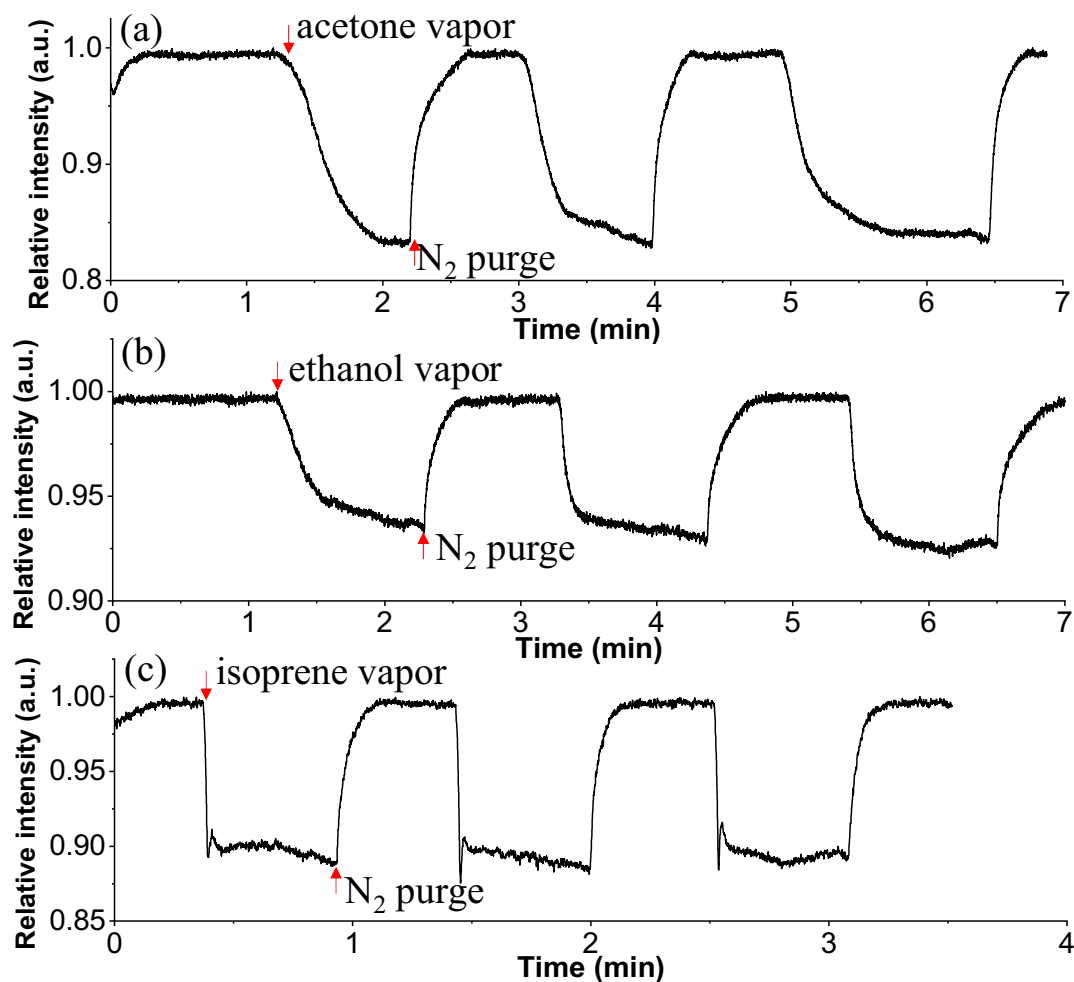
Figure 7. Real-time mid-IR monitoring of pulsed VOCs using SiN waveguides of width = 10 μm and thickness = 1 μm: (**a**) acetone at λ = 3.375 μm, (**b**) ethanol at λ = 3.375 μm, and (**c**) isoprene at λ = 3.400 μm.

absorption curve can be explained by a superposition of an adsorption isotherm and a linear adsorption increase caused by the non-adhesive analytes within the waveguide's evanescent field. Applying the Antoine equation, the concentration of the VOC acetone vapor is 10 mmol/L, equivalent to 24% at 1 atm[36]. Further, according to the Lambert–Beer's Law and using the sensitivity as defined in Ref.[38], the waveguide output intensity I can be derived from Eq. (1).

$$I = I_0 e^{-A} = I_0 e^{-\varepsilon \eta c l} \tag{1}$$

Here, I_0 is the waveguide output intensity without VOCs, A is the VOC absorbance, ε is the specific VOC absorption, η is the fraction of the evanescent power outside of the waveguide core, c is the VOC concentration, and l is the sensing length. The ultimate theoretical sensitivity of the waveguide is then defined in Eq. (2).

$$S = \frac{dI}{dc} = -I_0 \varepsilon \eta l e^{-\varepsilon \eta c l} \tag{2}$$

From the real-time measurement in Fig. 7, $A_{max} = -\log\left(\frac{I}{I_0}\right) = -\log\left(\frac{0.85}{1}\right) = 0.071$, which is the maximum absorbance upon exposure to the saturated acetone vapor. The noise equivalent power (NEP) of the mid-IR photodetector is 1.5×10^{-10} W/$\sqrt{\text{Hz}}$, and the responsivity is 3×10^3 V/W. The integration time is 35 μs, resulting in a bandwidth of $\Delta f = \frac{1}{2t_c} = 14$ kHz. Considering the above parameters, the noise level I_{noise} is ± 0.05 mV. Because the waveguide output intensity is higher than 100 mV, the ratio of the noise compared to the waveguide output intensity is 0.1%. Therefore, the signal fluctuation is mainly caused by the circuit noise from the photodetector. In addition, the signal to noise ratio should be at least 3 for a valid absorption measurement. This corresponds to a detectable signal change of $\Delta I = \pm 0.3\% I_0$ or a minimum detectable absorbance $A_{min} = -\log\left(\frac{I_0 - \Delta I}{I_0}\right) = 0.003$. Hence, the LOD of acetone is 1/20 × the saturated acetone vapor, equivalent to 1.2%. Considering Eq. (1), we found $\alpha = \varepsilon \eta l = \frac{A}{c} = 0.3$. Therefore, the sensitivity at the lowest concentration
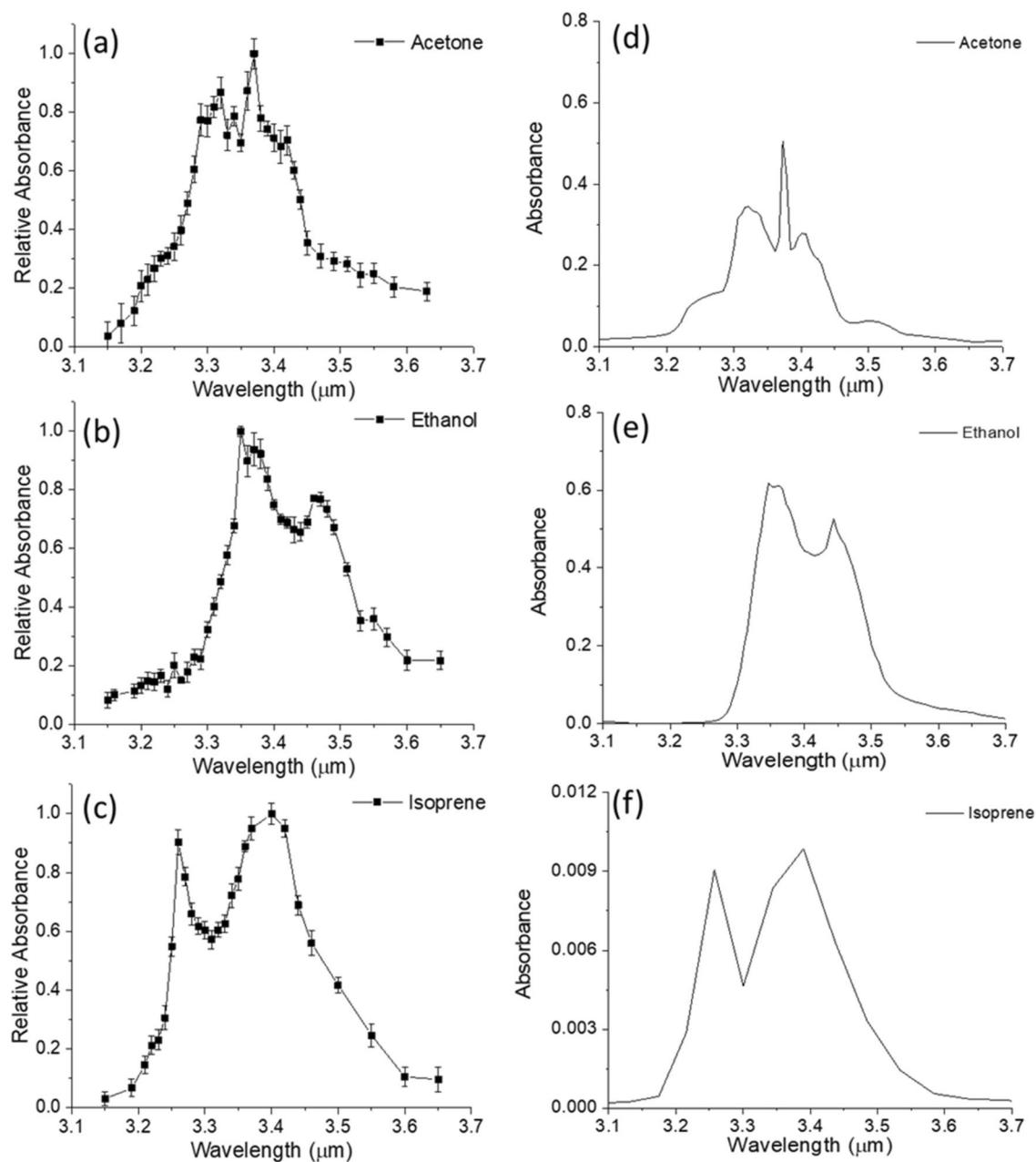
Figure 8. Mid-IR absorption spectra of acetone, ethanol, and isoprene. (**a–c**) Results from SiN waveguide measurement. (**d–f**) Spectra from the NIST WebBook database[35].

of 1.2% is 30 mV per unit concentration change. Using the same approach, the LOD of the concentration were 1.3% for ethanol and 2.5% for isoprene. The sensitivity of our mid-IR waveguide is better than the refractive-index-based sensing using a visible waveguide because of the strong characteristic mid-IR C–H vibrational absorption[37].

In the future, our waveguide sensitivity can be further increased with the use of slot waveguides and nanoparticles[39,40]. Specifically, our previous work has shown a 10–15 times enhancement of the sensitivity by coating nanoparticles on the device surface[41,42]. Further, compared to a ridge waveguide, a slot-waveguide can improve the sensitivity approaching 50 times. We expect that these advancements can enhance sensitivity by 500×, bringing it closer to that of MOS sensors, which achieve sub ppm levels, while still providing the advantage of better specificity. Thus, the potential for enhancement of sensitivity of waveguide-based sensing, taken together with intrinsically high, spectroscopic selectivity of mid-IR detection[43] make this approach promising for future sensing applications of multiple gaseous analytes.
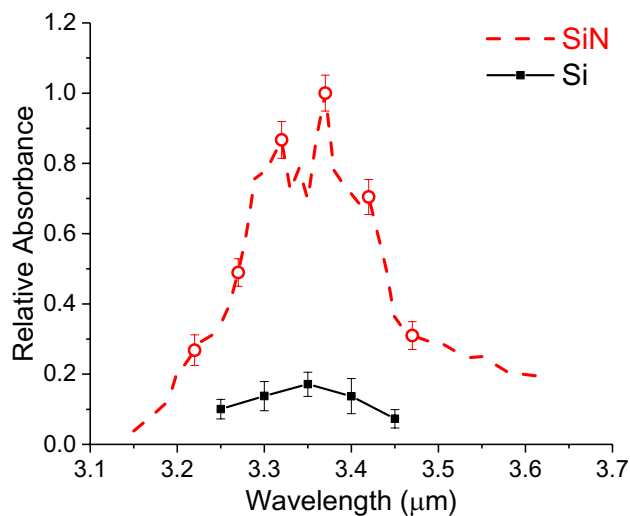
Figure 9. Measured results of acetone using SiN waveguides compared with Si waveguides. The waveguide width = 10 μm and thickness T = 1 μm.
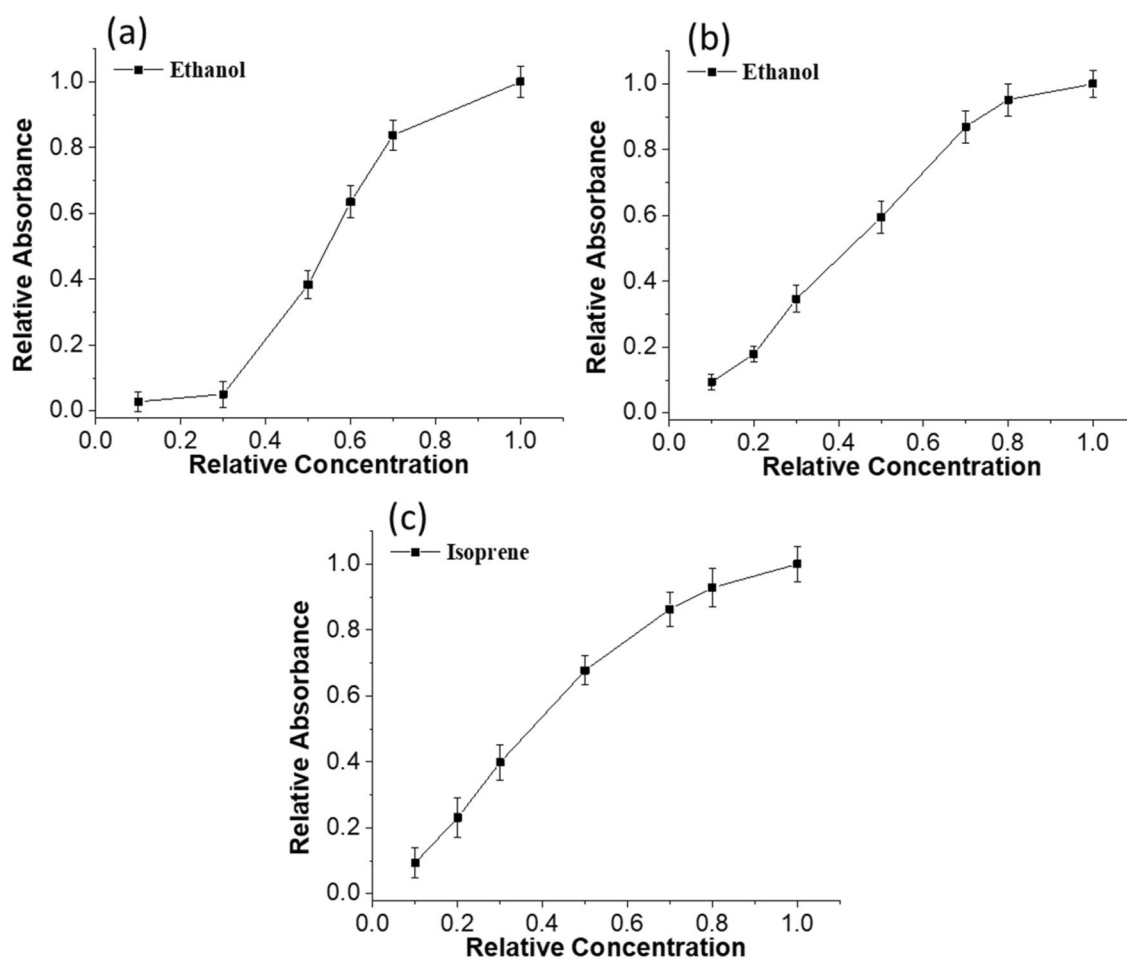

Figure 10. Relative absorbance vs relative VOC concentration for (**a**) acetone at λ = 3.375 μm, (**b**) ethanol at λ = 3.375 μm, and (**c**) isoprene at λ = 3.400 μm.

Conclusions

Mid-IR Si and SiN waveguide sensors were evaluated theoretically and experimentally as robust, chemically stable platforms for on-chip VOC detection. Utilizing the C–H stretching vibrational mid-IR region between 3.1 to 3.5 μm, acetone, ethanol, and isoprene vapors were detected in real time using both waveguides. We demonstrated that due to their low refractive index, SiN waveguides had five times higher sensitivity than Si waveguides, and unlike Si waveguides were able to resolve the mid-IR absorption spectra of VOCs in the entire C–H strength region. Because of its CMOS compatibility, the proposed waveguide sensor can be integrated with wireless electronics and potentially provide a compact module for sensing of gaseous analytes for health, agricultural and environmental applications.

References

1. Schnabel, R. *et al.* Analysis of volatile organic compounds in exhaled breath to diagnose ventilator-associated pneumonia. *Sci. Rep.* **5**, 1–10 (2015).
2. Ahmed, W. M. *et al.* Exhaled volatile organic compounds of infection: A systematic review. *ACS Infect. Dis.* **3**, 695–710 (2017).
3. Jansen, R. *et al.* Detection of diseased plants by analysis of volatile organic compound emission. *Annu. Rev. Phytopathol.* **49**, 157–174 (2011).
4. Li, Z. *et al.* Non-invasive plant disease diagnostics enabled by smartphone-based fingerprinting of leaf volatiles. *Nat. Plants* **5**, 856–866 (2019).
5. Cetin, E., Odabasi, M. & Seyfioglu, R. Ambient volatile organic compound (VOC) concentrations around a petrochemical complex and a petroleum refinery. *Sci. Total Environ.* **312**, 103–112 (2003).
6. Lamote, K. *et al.* Breath analysis by gas chromatography-mass spectrometry and electronic nose to screen for pleural mesothelioma: A cross-sectional case-control study. *Oncotarget* **8**, 91593 (2017).
7. Wang, X. R., Cassells, J. & Berna, A. Z. Stability control for breath analysis using GC-MS. *J. Chromatogr. B* **1097**, 27–34 (2018).
8. Masikini, M., Chowdhury, M. & Nemraoui, O. Metal oxides: Application in exhaled breath acetone chemiresistive sensors. *J. Electrochem. Soc.* **167**, 037537 (2020).
9. Righettoni, M., Amann, A. & Pratsinis, S. E. Breath analysis by nanostructured metal oxides as chemo-resistive gas sensors. *Mater. Today* **18**, 163–171 (2015).
10. Paul, R. K., Badhulika, S., Saucedo, N. M. & Mulchandani, A. Graphene nanomesh as highly sensitive chemiresistor gas sensor. *Anal. Chem.* **84**, 8171–8178 (2012).
11. Park, C.-O., Fergus, J., Miura, N., Park, J. & Choi, A. Solid-state electrochemical gas sensors. *Ionics* **15**, 261–284 (2009).
12. Marchi, I., Rudaz, S. & Veuthey, J.-L. Atmospheric pressure photoionization for coupling liquid-chromatography to mass spectrometry: A review. *Talanta* **78**, 1–18 (2009).
13. Henderson, B. *et al.* Laser spectroscopy for breath analysis: Towards clinical implementation. *Appl. Phys. B* **124**, 161 (2018).
14. Selvaraj, R., Vasa, N. J., Nagendra, S. & Mizaikoff, B. Advances in mid-infrared spectroscopy-based sensing techniques for exhaled breath diagnostics. *Molecules* **25**, 2227 (2020).
15. Lin, P. T. *et al.* Chip-scale Mid-Infrared chemical sensors using air-clad pedestal silicon waveguides. *Lab Chip* **13**, 2161–2166 (2013).
16. Su, P. *et al.* Monolithic on-chip mid-IR methane gas sensor with waveguide-integrated detector. *Appl. Phys. Lett.* **114**, 051103 (2019).
17. Kumari, B., Barh, A., Varshney, R. & Pal, B. Silicon-on-nitride slot waveguide: A promising platform as mid-IR trace gas sensor. *Sens. Actuators B Chem.* **236**, 759–764 (2016).
18. Jin, T., Zhou, J. & Lin, P. T. Real-time and non-destructive hydrocarbon gas sensing using mid-infrared integrated photonic circuits. *RSC Adv.* **10**, 7452–7459 (2020).
19. Chang, Y.-C. *et al.* Cocaine detection by a mid-infrared waveguide integrated with a microfluidic chip. *Lab Chip* **12**, 3020–3023 (2012).
20. Messica, A., Greenstein, A. & Katzir, A. Theory of fiber-optic, evanescent-wave spectroscopy and sensors. *Appl. Opt.* **35**, 2274–2284 (1996).
21. Pandraud, G. *et al.* Evanescent wave sensing: New features for detection in small volumes. *Sens. Actuators A Phys.* **85**, 158–162 (2000).
22. Jin, T., Zhou, J., Lin, H.-Y.G. & Lin, P. T. Mid-infrared chalcogenide waveguides for real-time and nondestructive volatile organic compound detection. *Anal. Chem.* **91**, 817–822 (2018).
23. Ebnesajjad, S. & Ebnesajjad, C. *Surface Treatment of Materials for Adhesive Bonding* (William Andrew, 2013).
24. Krstic, Z. & Krstic, V. D. Silicon nitride: The engineering material of the future. *J. Mater. Sci.* **47**, 535–552 (2012).
25. Lin, P. T., Singh, V., Kimerling, L. & Murthy Agarwal, A. Planar silicon nitride mid-infrared devices. *Appl. Phys. Lett.* **102**, 251121 (2013).
26. Lin, P. T. *et al.* Label-free glucose sensing using chip-scale mid-infrared integrated photonics. *Adv. Opt. Mater.* **4**, 1755–1759 (2016).
27. Koompai, N. *et al.* Analysis of Si3N4 waveguides for on-chip gas sensing by optical absorption within the mid-infrared region between 2.7 and 3.4 μm. *Results Phys.* **16**, 102957 (2020).
28. Antonacci, G. *et al.* Ultra-sensitive refractive index gas sensor with functionalized silicon nitride photonic circuits. *APL Photonics* **5**, 081301 (2020).
29. Chen, Y., Lin, H., Hu, J. & Li, M. Heterogeneously integrated silicon photonics for the mid-infrared and spectroscopic sensing. *ACS Nano* **8**, 6955–6961 (2014).
30. Righettoni, M. & Tricoli, A. Toward portable breath acetone analysis for diabetes detection. *J. Breath Res.* **5**, 037109 (2011).
31. Sun, M. *et al.* Study of breath acetone and its correlations with blood glucose and blood beta-hydroxybutyrate using an animal model with lab-developed type 1 diabetic rats. *RSC Adv.* **5**, 71002–71010 (2015).
32. Andresen-Streichert, H., Müller, A., Glahn, A., Skopp, G. & Sterneck, M. Alcohol biomarkers in clinical and forensic contexts. *Deutsch. Ärzteblatt Int.* **115**, 309 (2018).
33. Bajtarevic, A. *et al.* Noninvasive detection of lung cancer by analysis of exhaled breath. *BMC Cancer* **9**, 348 (2009).
34. Zhou, X. *et al.* Nanomaterial-based gas sensors used for breath diagnosis. *J. Mater. Chem. B* **8**, 3231–3248 (2020).
35. Coblentz Society, Inc. Evaluated infrared reference spectra. in *NIST Chemistry WebBook, NIST Standard Reference Database Number 69* (eds Linstrom, P. J. & Mallard, W. G.) 20899 (National Institute of Standards and Technology). https://doi.org/10.18434/T4D303 (retrieved November 8, 2020).
36. Yaws, C. L. *The Yaws Handbook of Vapor Pressure: Antoine Coefficients* (Gulf Professional Publishing, 2015).
37. Nitiss, E., Bundulis, A., Tokmakovs, A., Busenbergs, J. & Rutkis, M. All-organic waveguide sensor for volatile solvent sensing. *Photonic Sensors* **9**, 356–366 (2019).

38. Siebert, R. & Müller, J. Infrared integrated optical evanescent field sensor for gas analysis: Part II. Fabrication. *Sensors Actuators A Phys.* **119**, 584–592 (2005).
39. Al Husseini, D. *et al.* Surface functionalization utilizing mesoporous silica nanoparticles for enhanced evanescent-field mid-infrared waveguide gas sensing. *Coatings* **11**, 118 (2021).
40. Lin, P. T. *et al.* Mid-infrared spectrometer using opto-nanofluidic slot-waveguide for label-free on-chip chemical sensing. *Nano Lett.* **14**, 231–238 (2014).
41. Dey, A. Semiconductor metal oxide gas sensors: A review. *Mater. Sci. Eng. B* **229**, 206–217 (2018).
42. Zhang, J., Qin, Z., Zeng, D. & Xie, C. Metal-oxide-semiconductor based gas sensors: Screening, preparation, and integration. *Phys. Chem. Chem. Phys.* **19**, 6313–6329 (2017).
43. Al Husseini, D. *et al.* All-nanoparticle layer-by-layer coatings for Mid-IR on-chip gas sensing. *Chem. Commun.* **56**, 14283–14286 (2020).

Acknowledgements

Author contributions

J.Z., D.A.H., J.L., and Z.L. performed the experiments. S.S., G.L.C., R.G.O., and P.T.L. supervised the research. All authors reviewed the manuscript.

Competing interests

The authors declare no competing interests.

Additional information

Correspondence and requests for materials should be addressed to P.T.L.

Reprints and permissions information is available at www.nature.com/reprints.

Publisher's note Springer Nature remains neutral with regard to jurisdictional claims in published maps and institutional affiliations.